QCLAB++: Simulating Quantum Circuits on GPUs

Roel Van Beeumen[1], Daan Camps[2], Neil Mehta[2]

[1]Applied Mathematics and Computational Research Division, Lawrence Berkeley National Laboratory, Berkeley, CA, USA
[2]National Energy Research Scientific Computing Center, Lawrence Berkeley National Laboratory, Berkeley, CA, USA

Abstract

We introduce `qclab++`, a light-weight, fully-templated `C++` package for GPU-accelerated quantum circuit simulations. The code offers a high degree of portability as it has no external dependencies and the GPU kernels are generated through `OpenMP` offloading. `qclab++` is designed for performance and numerical stability through highly optimized gate simulation algorithms for 1-qubit, controlled 1-qubit, and 2-qubit gates. Furthermore, we also introduce `qclab` a quantum circuit toolbox for MATLAB with a syntax that mimics `qclab++`. This provides users the flexibility and ease of use of a scripting language like MATLAB for studying their quantum algorithms, while offering high-performance GPU acceleration when required. As such, the `qclab++` library offers a unique combination of features. We compare the CPU simulator in `qclab++` with the GPU kernels generated by `OpenMP` and observe a speedup of over $40\times$. Furthermore, we also compare `qclab++` to other circuit simulation packages, such as cirq-qsim and qibo, in a series of benchmarks conducted on NERSC's Perlmutter system and illustrate its competitiveness.

1 Introduction

The field of quantum computing is quickly progressing as is illustrated by recent developments in quantum hardware. Recent initial steps towards experimental realization of error correcting schemes in quantum processors based on superconducting [12] and ion traps [14] are encouraging milestones for the field. Other qubit modalities, such as neutral atoms [16], have also shown significant promise.

Most quantum hardware platforms that are currently being developed support a circuit model of quantum computation. It is thus of interest to the community of quantum algorithm researchers to have access to advanced computational tools that can help them in their research while quantum hardware is being developed. In addition to access to QPUs, quantum circuit simulators are of interest for a variety of reasons. First, it allows the researcher to prototype and investigate novel algorithms without using up valuable quantum resources for debugging and testing their ideas. This can instead all be done using simulations on classical hardware. Second, as the currently available quantum hardware is still suffering from noise, it is not possible to study algorithms that require a circuit depth that lies beyond the coherence limits of the device. Many algorithms of interest, for example in molecular sciences [10], require deep circuits.

This has sparked the development of multiple quantum simulators each with their own advantages and strengths. The *Cirq* toolbox [4] with the *qsim* simulator [13] is developed by Google Quantum AI, IBM has *Qiskit* [11] with the *Aer* simulator backend, and *PennyLane* [1] is a differentiable quantum programming framework from Xanadu. Similar efforts are pursued in *Qibo* [7, 6], which includes a JIT compiler for quantum simulation, and *Quest* [9]. All of the aforementioned packages, with the exception of Quest, provide a Python API to generate the quantum program.

Recently, NVIDIA has introduced their *cuQuantum* SDK [8] which offers a collection of GPU kernels to perform quantum gate simulations. Many existing quantum simulation packages, such as Cirq, Qiskit, PennyLane and Qibo, have started to support the cuQuantum SDK to run circuit simulations on NVIDIA hardware.

In this work, we introduce *two* alternative quantum circuit programming and simulation frameworks, called qclab++[1] [15] and qclab[2] [2]. The former is a light-weight fully-templated C++ library that supports GPU accelerated state vector simulations through OpenMP offloading, while the latter is a MATLAB toolbox that has an accessible interface that makes use of the advantages the MATLAB IDE offers. Both libraries provide a similar programming interface, see Figure 1, which lowers the barrier for converting simulation codes from one framework to the other and allows for a streamlined workflow where ideas are first prototyped in MATLAB and later simulated at larger scale on the GPU with qclab++. As an example, we illustrate this for the QFT circuit [5, 3] in Fig. 1. Remark that both implementations are very similar and easy to convert into each other.

```matlab
% number of qubits
n = 5;

% quantum circuit
circ = qclab.QCircuit(n);

% blocks
for i=0:n-1
  % Hadamard
  circ.push_back( H(i) );
  % diagonal blocks
  for j=2:n-i
    ctrl = j+i-1;
    th = -2*pi/2^j;
    circ.push_back( ...
      CP(ctrl, i, 1, th) );
  end
end

% swaps
for i=0:floor(n/2)-1
  circ.push_back( ...
    SWAP(i, n-i-1) );
end
```

```cpp
// number of qubits
int n = 5 ;

// quantum circuit
qclab::QCircuit<std::complex<double>> circ(n);

// blocks
for (int i=0; i<n; i++) {
  // Hadamard
  circ.push_back( std::make_unique<H>(i) );
  // diagonal blocks
  for (int j=2; j<=n-i; j++) {
    int ctrl = j+i-1;
    double th = -2*pi/(1<<j);
    circ.push_back(
      std::make_unique<CP>(ctrl, i, th) );
  }
}

// swaps
for (int i=0; i<n/2; i++) {
  circ.push_back(
    std::make_unique<SWAP>(i, n-i-1) );
}
```

Figure 1: MATLAB implementation of the QFT circuit [5, 3] with the qclab toolbox (*left*) and equivalent C++ implementation using qclab++ (*right*).

Our simulators are *strong* simulators that keep track of all amplitudes in the wavefunction as it is modified by the quantum circuit. This simulation problem naturally scales exponentially in the number of qubits of the quantum system and linearly in the number of gates in the circuit. The main advantages of strong simulation is that we have access to every amplitude at each step of the simulation and that all computations are exact up to numerical precision. The main disadvantage is that the wavefunction scales exponentially and this imposes a limit on the size of system one can simulate classically. This limit is in the range of 40-50 qubits. Approximate simulation methods using tensor network or sparse representation of the wave function can scale to larger systems but cannot approximate every state in Hilbert space up to the same accuracy.

The remainder of this paper is organized as follows. In Section 2, we describe the optimized

---

[1] qclab++: https://github.com/QuantumComputingLab/qclabpp
[2] qclab: https://github.com/QuantumComputingLab/qclab

state vector simulator algorithms for 1-qubit, controlled 1-qubit, and 2-qubit gates. In Section 3, we discuss the implementation details and the `OpenMP` offloading used to accelerate `qclab++`. In Section 4, we compare the CPU and GPU implementations of `qclab++` and benchmark it with other GPU-accelerated state vector simulation packages.

2 Efficient quantum gate simulations

The application of a unitary quantum gate U to a given state $|\phi\rangle \in \mathbb{C}^{2^n}$ (Fig. 2) corresponds mathematically to the matrix-vector multiplication (*matvec*)

$$|\psi\rangle = (I_l \otimes U \otimes I_r) |\phi\rangle, \tag{1}$$

where $\otimes$ denotes the Kronecker product and I_l, I_r are identity matrices of appropriate dimensions. A naive implementation of quantum circuit simulator would carry out the Kronecker products of (1) explicitly, and require 2 nested for loops.
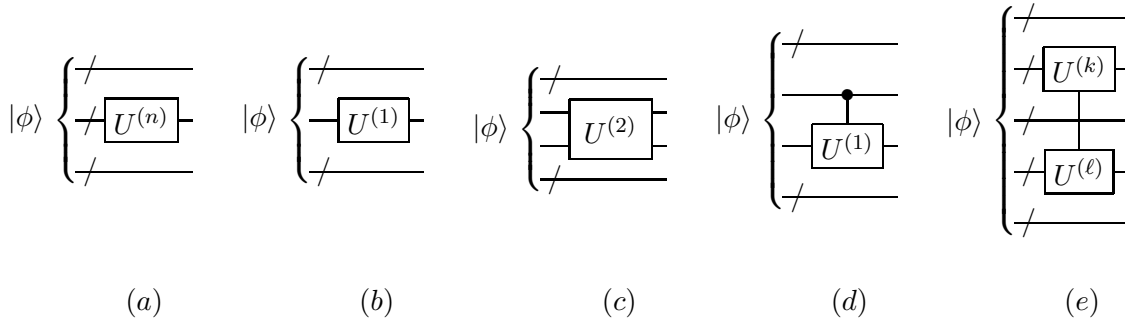

$$(a) \qquad\qquad (b) \qquad\qquad (c) \qquad\qquad (d) \qquad\qquad (e)$$

Figure 2: Application of (a) a dense n-qubit quantum gate, (b) a 1-qubit quantum gate, (c) a 2-qubit quantum gate, (d) a controlled 1-qubit quantum gate, and (e) a $k + \ell$ quantum gate acting on noncontiguous qubits to a quantum state $|\phi\rangle$.

In this section, we introduce more efficient algorithms for quantum gate simulation that only consist of 1 simple for loop combined with bit operations for index calculations. We therefore will use the *big-endian* binary convention as given by the following definition.

Definition 1 (Binary representation). *We define the binary representation of $j \in \mathbb{N} : 0 \leq j \leq 2^n - 1$ as follows*

$$j = [\mathtt{j_0 j_1 \cdots j_{n-1}}] = \mathtt{j_0} \cdot 2^{n-1} + \mathtt{j_1} \cdot 2^{n-2} + \cdots + \mathtt{j_{n-1}} \cdot 2^0,$$

where $\mathtt{j}_i \in \{0, 1\}$ for $i = 0, \ldots, n - 1$.

2.1 1-qubit gates

We start with the simplest class of quantum gates that only act on a single qubit

$$U := \begin{bmatrix} u_{0,0} & u_{0,1} \\ u_{1,0} & u_{1,1} \end{bmatrix}. \tag{2}$$

As illustrated by the different colors in Fig. 3, the state vector simulation of a 1-qubit gate breaks down in a series of 2×2 matvec operations

$$\begin{bmatrix} \psi_{\mathtt{i_0 i_1 \cdots i_{q-1} 0 i_{q+1} \cdots i_{n-1}}} \\ \psi_{\mathtt{i_0 i_1 \cdots i_{q-1} 1 i_{q+1} \cdots i_{n-1}}} \end{bmatrix} = \begin{bmatrix} u_{0,0} & u_{0,1} \\ u_{1,0} & u_{1,1} \end{bmatrix} \begin{bmatrix} \phi_{\mathtt{i_0 i_1 \cdots i_{q-1} 0 i_{q+1} \cdots i_{n-1}}} \\ \phi_{\mathtt{i_0 i_1 \cdots i_{q-1} 1 i_{q+1} \cdots i_{n-1}}} \end{bmatrix}, \tag{3}$$

$$a_j = [\,0\,\mathtt{i_0 i_1}\,] \quad\to\quad \{0,1,2,3\}$$
$$b_j = [\,1\,\mathtt{i_0 i_1}\,] \quad\to\quad \{4,5,6,7\}$$

$$m_L = 0 \quad\to\quad [0\cdots 0\,00]$$
$$m_R = 3 \quad\to\quad [0\cdots 0\,11]$$

$$a_j = [\,\mathtt{i_0}\,0\,\mathtt{i_1}\,] \quad\to\quad \{0,1,4,5\}$$
$$b_j = [\,\mathtt{i_0}\,1\,\mathtt{i_1}\,] \quad\to\quad \{2,3,6,7\}$$

$$m_L = 2 \quad\to\quad [0\cdots 0\,10]$$
$$m_R = 1 \quad\to\quad [0\cdots 0\,01]$$

$$a_j = [\,\mathtt{i_0 i_1}\,0\,] \quad\to\quad \{0,2,4,6\}$$
$$b_j = [\,\mathtt{i_0 i_1}\,1\,] \quad\to\quad \{1,3,5,7\}$$

$$m_L = 3 \quad\to\quad [0\cdots 0\,11]$$
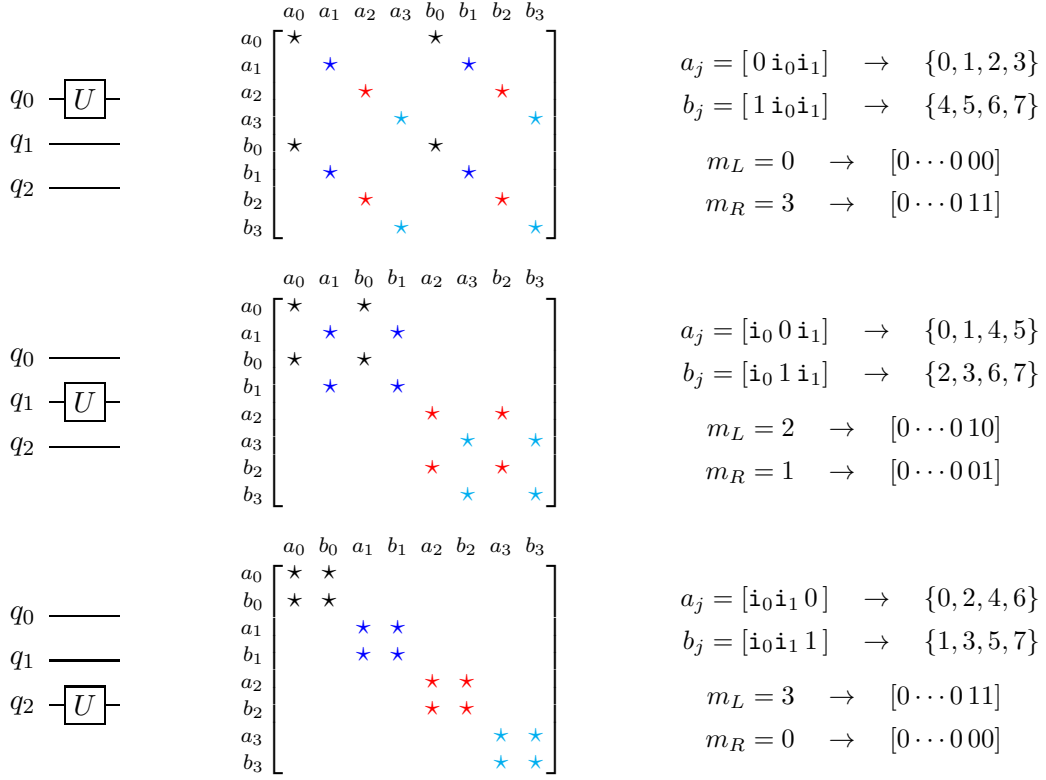$$m_R = 0 \quad\to\quad [0\cdots 0\,00]$$

Figure 3: Graphical illustration of applying a 1-qubit gate U.

where q is the qubit the gate U is acting on. Depending on q, the indices in (3)

$$
\begin{aligned}
[\mathtt{i_0 i_1} \cdots \mathtt{i_{q-1}}\, 0\, \mathtt{i_{q+1}} \cdots \mathtt{i_{n-1}}] &=: a_j, \\
[\mathtt{i_0 i_1} \cdots \mathtt{i_{q-1}}\, 1\, \mathtt{i_{q+1}} \cdots \mathtt{i_{n-1}}] &=: b_j,
\end{aligned}
\qquad j = 0,1,\ldots,2^{n-1}-1, \qquad (4)
$$

can be next to each other or separated up to 2^{n-1}. We will now describe an efficient way to calculate (4) solely based on bit operations.

First, we observe that the binary representations of a_j and b_j can be split into 3 parts, i.e., the bits left of 0 (and 1), the 0 (and 1) bit, and the bits right of 0 (and 1), respectively. Without loss of generality, we can select the bits $\mathtt{i_\ell}$ for $0 \le \ell \le n-1$ and $\ell \ne q$, so that

$$ j = [\mathtt{i_0 i_1} \cdots \mathtt{i_{q-1}} \,|\, \mathtt{i_{q+1}} \cdots \mathtt{i_{n-1}}]. \qquad (5) $$

Next, using the following left and right bit masks

$$ m_L := [0\cdots 0\,|\,\overbrace{1\cdots 1}^{q}\,|\,0\cdots 0] = \left(2^{n-1}-1\right) - \left(2^{n-q-1}-1\right), \qquad (6) $$
$$ m_R := [0\cdots 0\,|\,0\cdots 0\,|\,\underbrace{1\cdots 1}_{n-q-1}] = 2^{n-q-1}-1, \qquad (7) $$

we can compute each a_j as the sum of j masked with m_R and a left shift of j masked with m_L,

$$ a_j = (j\,\&\,m_R) + [(j\,\&\,m_L) \ll 1], \qquad (8) $$

4

and the corresponding b_j index results from the following sum

$$b_j = a_j + 2^{n-q-1}. \tag{9}$$

The algorithm for the vector simulation of a general 1-qubit gate is given in Algorithm 1. Note that for 1-qubit gates with some of the elements in (2) equal to 0, Lines 5 and 6 can be simplified. For example, the Pauli-X gate is just a swap operation

$$\psi[a_j] = \phi[b_j],$$
$$\psi[b_j] = \phi[a_j],$$

and the Pauli-Y gate

$$\psi[a_j] = -i\phi[b_j],$$
$$\psi[b_j] = i\phi[a_j].$$

Remark that for the Pauli-Z gate only half of the vector elements (b_j) need to be updated

$$\psi[a_j] = \phi[a_j],$$
$$\psi[b_j] = -\phi[b_j].$$

Algorithm 1: Apply 1-qubit gate

Input: Input state $|\phi\rangle$.
Output: Output state $|\psi\rangle = U|\phi\rangle$.

1   Right mask: $m_R = 2^{n-q-1} - 1$
2   Left mask: $m_L = 2^{n-1} - 1 - m_R$
   for $j = 0, 1, \ldots, 2^{n-1} - 1$ **do**
3      $a_j = (j \,\&\, m_R) + [(j \,\&\, m_L) \ll 1]$
4      $b_j = a_j + 2^{n-q-1}$
5      $\psi[a_j] = u_{0,0}\phi[a_j] + u_{0,1}\phi[b_j]$
6      $\psi[b_j] = u_{1,0}\phi[a_j] + u_{1,1}\phi[b_j]$
   end

2.2   Controlled 1-qubit gates

We now consider the controlled 1-qubit gates and distinguish the following 4 different cases

$$\tag{10}$$

where q_c is the control qubit and q_t the target qubit. As illustrated in Fig. 4, these controlled gates only update half of the elements. Which elements are updated depend on the actual values of the q_c and q_t.

Similar to the standard 1-qubit gate, the state vector simulation of a controlled 1-qubit gate breaks down in a series of 2×2 matvec operations

$$\begin{bmatrix} \psi_{a_j} \\ \psi_{b_j} \end{bmatrix} = \begin{bmatrix} u_{0,0} & u_{0,1} \\ u_{1,0} & u_{1,1} \end{bmatrix} \begin{bmatrix} \phi_{a_j} \\ \phi_{b_j} \end{bmatrix}, \tag{11}$$

q_0 —●—
q_1 —U—
q_2 ————

$$
\begin{array}{c}
a_0\ \ a_1\ \ b_0\ \ b_1\\
\begin{array}{c}\\\\\\\\a_0\\a_1\\b_0\\b_1\end{array}
\left[\begin{array}{cccccccc}
1\\
&1\\
&&1\\
&&&1\\
&&&&\star&&\star\\
&&&&&\star&&\star\\
&&&&\star&&\star\\
&&&&&\star&&\star
\end{array}\right]
\end{array}
$$

$a_j = [\underline{1}\,0\,\mathtt{i}_0] \quad\rightarrow\quad \{4,5\}$
$b_j = [\underline{1}\,1\,\mathtt{i}_0] \quad\rightarrow\quad \{6,7\}$

q_0 —○—
q_1 —U—
q_2 ————

$$
\begin{array}{c}
a_0\ \ a_1\ \ b_0\ \ b_1\\
\begin{array}{c}a_0\\a_1\\b_0\\b_1\\\\\\\\\end{array}
\left[\begin{array}{cccccccc}
\star&&\star\\
&\star&&\star\\
\star&&\star\\
&\star&&\star\\
&&&&1\\
&&&&&1\\
&&&&&&1\\
&&&&&&&1
\end{array}\right]
\end{array}
$$

$a_j = [\underline{0}\,0\,\mathtt{i}_0] \quad\rightarrow\quad \{0,1\}$
$b_j = [\underline{0}\,1\,\mathtt{i}_0] \quad\rightarrow\quad \{2,3\}$

q_0 ————
q_1 —U—
q_2 —●—

$$
\begin{array}{c}
a_0\ \ \ b_0\ \ \ a_1\ \ \ b_1\\
\begin{array}{c}\\a_0\\b_0\\\\a_1\\\\b_2\end{array}
\left[\begin{array}{cccccccc}
1\\
&\star&&\star\\
&&1\\
&\star&&\star\\
&&&&1\\
&&&&&\star&&\star\\
&&&&&&1\\
&&&&&\star&&\star
\end{array}\right]
\end{array}
$$

$a_j = [\mathtt{i}_0\,0\,\underline{1}] \quad\rightarrow\quad \{1,5\}$
$b_j = [\mathtt{i}_0\,1\,\underline{1}] \quad\rightarrow\quad \{3,7\}$

q_0 ————
q_1 —U—
q_2 —○—

$$
\begin{array}{c}
a_0\ \ \ b_0\ \ \ a_1\ \ \ b_1\\
\begin{array}{c}a_0\\\\b_0\\\\a_1\\\\b_1\end{array}
\left[\begin{array}{cccccccc}
\star&&\star\\
&1\\
\star&&\star\\
&&&1\\
&&&&\star&&\star\\
&&&&&1\\
&&&&\star&&\star\\
&&&&&&&1
\end{array}\right]
\end{array}
$$

$a_j = [\mathtt{i}_0\,0\,\underline{0}] \quad\rightarrow\quad \{0,4\}$
$b_j = [\mathtt{i}_0\,1\,\underline{0}] \quad\rightarrow\quad \{2,6\}$

Figure 4: Graphical illustration of applying a controlled 1-qubit gate U.

where we distinguish between the 2 left cases of (10), i.e., $q_c < q_t$,

$$
\begin{aligned}
a_j &= [\mathtt{i}_0\mathtt{i}_1\cdots\mathtt{i}_{q_c-1}*\mathtt{i}_{q_c+1}\cdots\mathtt{i}_{q_t-1}\,0\,\mathtt{i}_{q_t+1}\cdots\mathtt{i}_{n-1}],\\
b_j &= [\mathtt{i}_0\mathtt{i}_1\cdots\mathtt{i}_{q_c-1}*\mathtt{i}_{q_c+1}\cdots\mathtt{i}_{q_t-1}\,1\,\mathtt{i}_{q_t+1}\cdots\mathtt{i}_{n-1}],
\end{aligned} \qquad j = 0,1,\ldots,2^{n-2}-1, \qquad (12)
$$

and the 2 right cases of (10), i.e., $q_t < q_c$,

$$
\begin{aligned}
a_j &= [\mathtt{i}_0\mathtt{i}_1\cdots\mathtt{i}_{q_t-1}\,0\,\mathtt{i}_{q_t+1}\cdots\mathtt{i}_{q_c-1}*\mathtt{i}_{q_c+1}\cdots\mathtt{i}_{n-1}],\\
b_j &= [\mathtt{i}_0\mathtt{i}_1\cdots\mathtt{i}_{q_t-1}\,1\,\mathtt{i}_{q_t+1}\cdots\mathtt{i}_{q_c-1}*\mathtt{i}_{q_c+1}\cdots\mathtt{i}_{n-1}],
\end{aligned} \qquad j = 0,1,\ldots,2^{n-2}-1, \qquad (13)
$$

with $* = 0$ for zero-controlled gates and $* = 1$ for one-controlled gates. Note that we only have 2^{n-2} different values for j in contrast to 2^{n-1} values for the standard 1-qubit gate in (4).

Let

$$q_0 = \min(q_c, q_t), \qquad (14)$$
$$q_1 = \max(q_c, q_t). \qquad (15)$$

such that $q_0 < q_1$. Next, we observe that the indices a_j and b_j in (12) and (13) can be split into 5 parts. Without loss of generality, we can select the bits $\mathtt{i}_\ell$ for $0 \leq \ell \leq n-1$ and $\ell \neq \{q_0, q_1\}$, so that

$$j = [\mathtt{i}_0 \mathtt{i}_1 \cdots \mathtt{i}_{q_0-1} \,|\, \mathtt{i}_{q_0+1} \cdots \mathtt{i}_{q_1-1} \,|\, \mathtt{i}_{q_1+1} \cdots \mathtt{i}_{n-1}]. \tag{16}$$

Next, using the following bit masks

$$m_L := [0 \cdots 0 \,|\, \overbrace{1 \cdots 1}^{q_0} \,|\, \overbrace{0 \cdots 0}^{q_1-q_0-1} \,|\, 0 \cdots 0] = \left(2^{n-2} - 1\right) - \left(2^{n-q_0-2} - 1\right), \tag{17}$$

$$m_C := [0 \cdots 0 \,|\, 0 \cdots 0 \,|\, 1 \cdots 1 \,|\, 0 \cdots 0] = \left(2^{n-q_0-2} - 1\right) - \left(2^{n-q_1-1} - 1\right), \tag{18}$$

$$m_R := [0 \cdots 0 \,|\, 0 \cdots 0 \,|\, 0 \cdots 0 \,|\, \underbrace{1 \cdots 1}_{n-q_1-1}] = 2^{n-q_1-1} - 1, \tag{19}$$

we can compute the zero-controlled a_j indices as the sum of the following 3 terms

$$a_j = (j \,\&\, m_R) + [(j \,\&\, m_C) \ll 1] + [(j \,\&\, m_L) \ll 2], \tag{20}$$

and the corresponding b_j indices result from the following sum

$$b_j = a_j + 2^{n-q_t-1}. \tag{21}$$

In the case of a one-controlled gate, we need to increment both (20) and (21) by 2^{n-q_c-1}.

The algorithm for the vector simulation of a controlled 1-qubit gate is given in Algorithm 2. Similar to standard 1-qubit gates, controlled 1-qubit gates with some zero elements in (2), Lines 8 and 9 can be simplified. For example, the CNOT gate just swaps half of the elements.

Algorithm 2: Apply controlled 1-qubit gate

Input: Input state $|\phi\rangle$.
Output: Output state $|\psi\rangle = U |\phi\rangle$.

1 Right mask: $m_R = 2^{n-q_1-1} - 1$
2 Center mask: $m_C = 2^{n-q_0-2} - 1 - m_R$
3 Left mask: $m_L = 2^{n-2} - 1 - m_R - m_C$
   for $j = 0, 1, \ldots, 2^{n-2} - 1$ **do**
4     $a_j = (j \,\&\, m_R) + [(j \,\&\, m_C) \ll 1] + [(j \,\&\, m_L) \ll 2]$
5     $b_j = a_j + 2^{n-q_t-1}$
     if *control state = 1* **then**
6        $a_j = a_j + 2^{n-q_c-1}$
7        $b_j = b_j + 2^{n-q_c-1}$
     end
8     $\psi[a_j] = u_{0,0}\phi[a_j] + u_{0,1}\phi[b_j]$
9     $\psi[b_j] = u_{1,0}\phi[a_j] + u_{1,1}\phi[b_j]$
   end

2.3   2-qubit gates

The state vector simulation of general 2-qubit gates acting on qubits q_0 and q_1 breaks down in a series of 4×4 matvec operations. For the index calculations we can again make use of the bit mask (17)–(19) and the corresponding algorithm is given in Algorithm 3.

Algorithm 3: Apply 2-qubit gate

Input: Input state $|\phi\rangle$.
Output: Output state $|\psi\rangle = U |\phi\rangle$.

1 Right mask: $m_R = 2^{n-q_1-1} - 1$
2 Center mask: $m_C = 2^{n-q_0-2} - 1 - m_R$
3 Left mask: $m_L = 2^{n-2} - 1 - m_R - m_C$

  for $j = 0, 1, \ldots, 2^{n-2} - 1$ **do**

4 $a_j = (j \,\&\, m_R) + [(j \,\&\, m_C) \ll 1] + [(j \,\&\, m_L) \ll 2]$
5 $b_j = a_j + 2^{n-q_0-1}$
6 $c_j = a_j + 2^{n-q_1-1}$
7 $d_j = a_j + 2^{n-q_0-1} + 2^{n-q_1-1}$
8 $\psi[a_j] = u_{0,0}\phi[a_j] + u_{0,1}\phi[b_j] + u_{0,2}\phi[c_j] + u_{0,3}\phi[d_j]$
9 $\psi[b_j] = u_{1,0}\phi[a_j] + u_{1,1}\phi[b_j] + u_{1,2}\phi[c_j] + u_{1,3}\phi[d_j]$
10 $\psi[c_j] = u_{2,0}\phi[a_j] + u_{2,1}\phi[b_j] + u_{2,2}\phi[c_j] + u_{2,3}\phi[d_j]$
11 $\psi[d_j] = u_{3,0}\phi[a_j] + u_{3,1}\phi[b_j] + u_{3,2}\phi[c_j] + u_{3,3}\phi[d_j]$

  end

A particular and commonly used 2-qubit gate is the SWAP gate

$$U = \begin{bmatrix} 1 & 0 & 0 & 0 \\ 0 & 0 & 1 & 0 \\ 0 & 1 & 0 & 0 \\ 0 & 0 & 0 & 1 \end{bmatrix}. \tag{22}$$

In this case, the 4×4 operation corresponds to just swapping 2 elements. Hence, Lines 8 to 11 in Algorithm 3 yield

$$\begin{aligned} \psi[a_j] &= \phi[a_j], \\ \psi[b_j] &= \phi[c_j], \\ \psi[c_j] &= \phi[b_j], \\ \psi[d_j] &= \phi[d_j]. \end{aligned}$$

We remark that Algorithm 3 allows to apply arbitrary 2-qubit gates to noncontiguous qubits as illustrated in Fig. 2(e).

2.4 Multi-qubit gates

The algorithms for state vector simulation of 1- and 2-qubit gates can be generalized to multi-qubit gates in a straightforward manner. For every additional qubit, we need to define 2 additional bit masks to efficiently calculate the indices via bit operations.

However, the case of multi-controlled versions of smaller 1- or 2-qubit gates provides the most opportunity for performance gains. This is due to the fact that every additional control qubit halves the number of elements in the state vector that need to be updated. For example, as illustrated in Fig. 5, a doubly-controlled 1-qubit gate only updates 1/4 of the elements in the state vector. The Toffoli gate, or doubly-controlled NOT gate is the most common multi-qubit gate. Its implementation can be further optimized by swapping the elements of the state vector it acts on.
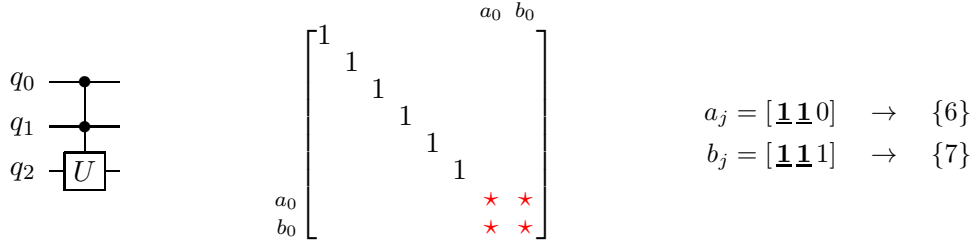
Figure 5: Graphical illustration of applying a double controlled 1-qubit gate U.

3 Implementation details

`qclab++` is an object-oriented, fully templated `C++` package for creating and representing quantum circuits. `qclab++` can be used for rapid prototyping and testing of quantum algorithms, and allows for fast algorithm development and discovery. `qclab++` has no external dependencies and provides I/O through openQASM making it compatible with quantum hardware.

In order to keep `qclab++` light-weighted and with a high degree of portability, all parallelization (both CPU and GPU) is done through `OpenMP`. Another advantage of `OpenMP` GPU offloading is that the CPU and GPU implementations of the algorithms in Section 2 are exactly the same except for the `OpenMP` `#pragma` statements. This is illustrated in Fig. 6 which shows the CPU and GPU implementations for applying the Pauli-X gate. Note that both implementations only differ in the `#pragma` statement above the for loop and the remaining part of the code is identical.

```
template <typename T>
void apply(int nbQubits, int qubit, T* x) {

  // number of iterations
  int jmax = 1 << (nbQubits-1);

  // bit masks
  int mR = (1 << (nbQubits-qubit-1)) - 1;
  int mL = (1 << (nbQubits-1)) - 1 - mR;

  // loop over 2x2 matvecs
  #pragma omp parallel for
  for (int j = 0; j < jmax; j++) {
    int aj = (j & mR) + ((j & mL) << 1);
    int bj = aj + 1 << (nbQubits-qubit-1);
    std::swap(x[aj], x[bj]);
  }

}
```

```
template <typename T>
void apply_device(int nbQubits, int qubit, T* x) {

  // number of iterations
  int jmax = 1 << (nbQubits-1);

  // bit masks
  int mR = (1 << (nbQubits-qubit-1)) - 1;
  int mL = (1 << (nbQubits-1)) - 1 - mR;

  // loop over 2x2 matvecs
  #pragma omp target teams distribute parallel for
  for (int j = 0; j < jmax; j++) {
    int aj = (j & mR) + ((j & mL) << 1);
    int bj = aj + 1 << (nbQubits-qubit-1);
    std::swap(x[aj], x[bj]);
  }

}
```

Figure 6: CPU (*left*) versus GPU (*right*) implementation of the Pauli-X gate in `qclab++`. Remark that they only differ in the `#pragma` statement above the for loop.

4 Numerical experiments

All experiments presented in this section where performed on the NERSC Perlmutter supercomputer. Each GPU node in Perlmutter is equipped with 4 NVIDIA A100 40GB GPUs and an AMD

EPYC 7763 CPU. The nodes are connected through a HPE Slingshot-11 interconnect. A single GPU has enough memory to store a 31 qubit state vector in complex double precision or a 32 qubit state vector in complex single precision. We first compare the `qclab++` CPU implementation to its GPU implementation. Next, we benchmark `qclab++` to other existing GPU-accelerated state vector simulation packages, such as cirq-qsim with the cuQuantum backend, and qibo both with the cupy and cuQuantum backends.

We select two scalable classes of benchmarking circuits to run our experiments on, see Fig. 7. The first is the QFT circuit, which consists of single qubit Hadamard gates, controlled phase gates that connect every pair of qubits in the circuit, and ends with a series of SWAP gates. The second circuit is a Trotter time evolution circuit for a 1D nearest-neighbor TFXY spin chain. This circuit consist of layers of single qubit rotations interleaved with leayers of CNOT gates acting on nearest-neighbor qubits.
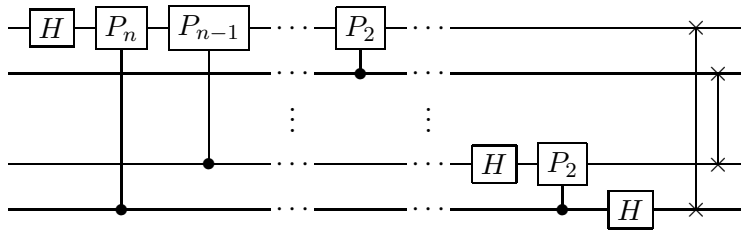
(a) QFT circuit
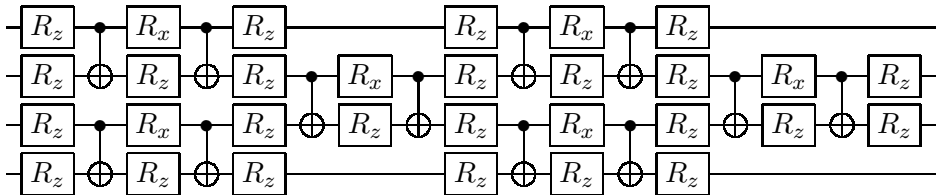
(b) Hamiltonian simulation circuit

Figure 7: Overview of the circuits used to benchmark the various quantum circuit simulators.

4.1 `qclab++`: CPU versus GPU

In a first experiment, we compare the CPU and GPU implementations in `qclab++`. The timinig results for the QFT and Hamiltonian simulation circuits are presented in Figs. 8 and 9, respectively. Both figures show timings and speedup factors for single and double precision.

We observe that the GPU kernels exhibit a perfect linear scaling on the loglog plot for systems with more than 22 qubits. Every additional qubit doubles the simulation time. The CPU simulation exhibits less regular scaling in the timings, likely due to memory access effects such as NUMA domains. Furthermore, the GPU simulation significantly outperforms the CPU implementation leading to speedup factors of over $40\times$. Note that the results are qualitatively comparable for both sets of benchmarking circuits. The main difference is that the Hamiltonian simulation circuit shows larger GPU speedups in the 19-25 qubit range compared to the QFT circuit.
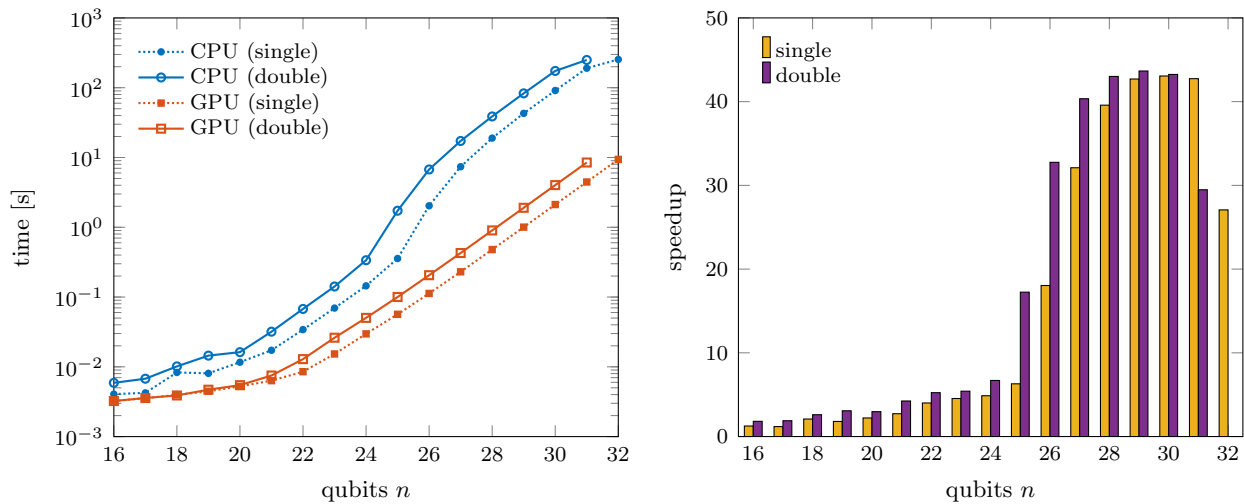
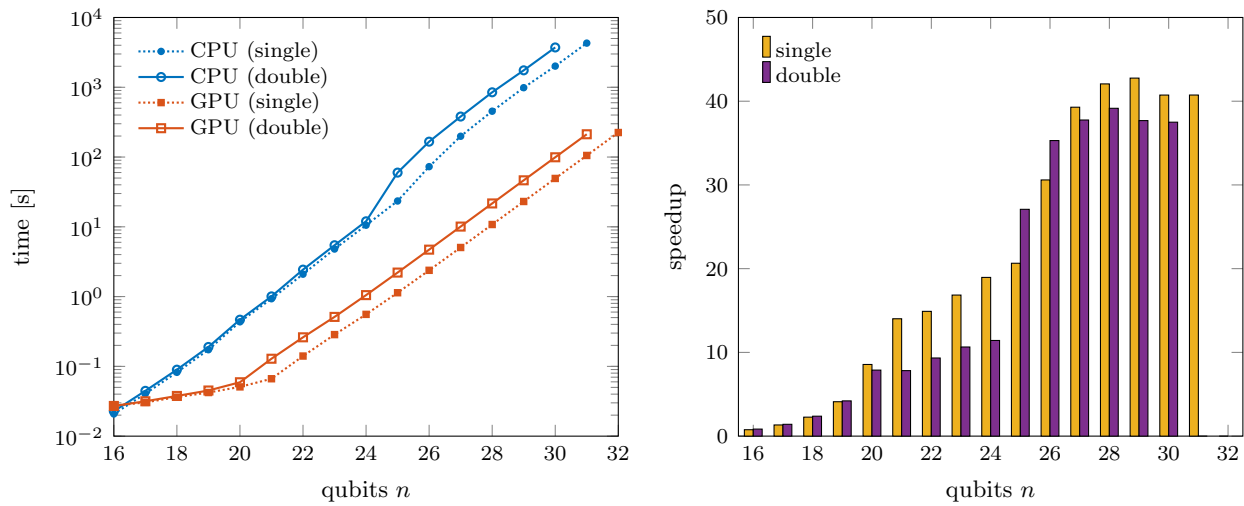Figure 8: `qclab++`: CPU versus GPU for QFT circuit (Perlmutter).

Figure 9: `qclab++`: CPU versus GPU for Hamiltonian simulation circuit (Perlmutter).

11

4.2 GPU benchmarking

In our second experiment, we compare the GPU state vector simulator of `qclab++` to the cuQuantum backend provided by cirq-qsim and to qibo, where we use both the cupy and cuQuantum backends. The timings for the single precision simulations are summarized in Fig. 10. The most notable difference appears in the smaller qubit regime, 16-25 qubits for the QFT circuit and 16-21 qubits for the Hamiltonian simulation circuit, where `qclab++` shows a signficant advantage over the other simulators. The most likely reason for this difference is that `qclab++` runs a compiled `C++` code which has a lower overhead compared to the Python interfaces the other simulators use. At the larger qubit sizes, the cost of the Python overhead becomes negligible and all simulators deliver a similar performance. We conclude that `qclab++` is competitive with other simulators while offering some distinct advantages.
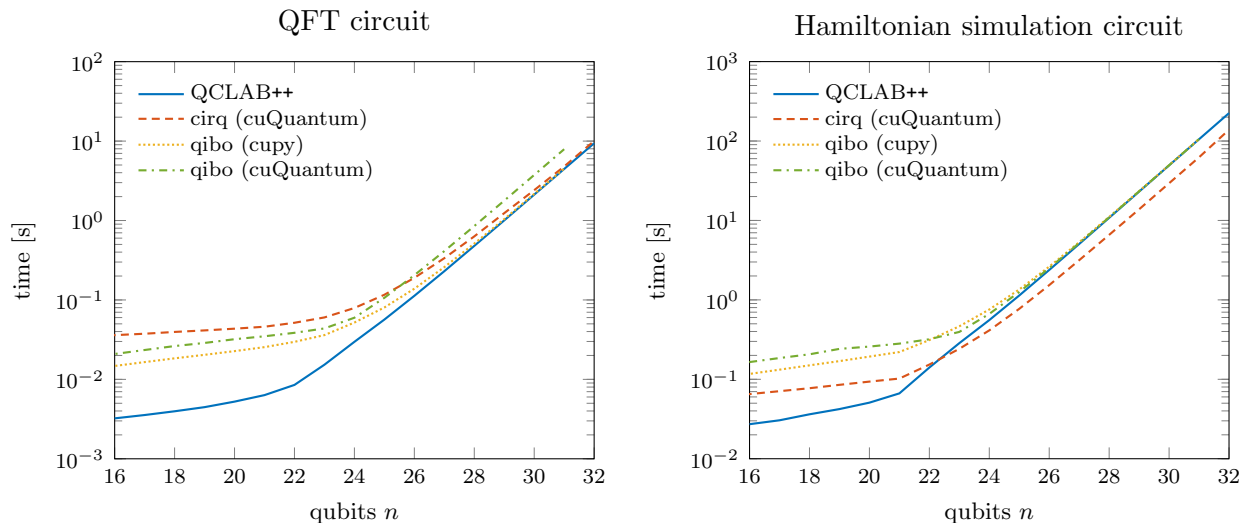

Figure 10: GPU benchmarking on Perlmutter (single precision).

Acknowledgements

References

[1] V. Bergholm et al. Pennylane: Automatic differentiation of hybrid quantum-classical computations, 2018. doi:10.48550/arXiv.1811.04968.

[2] D. Camps and R. Van Beeumen. Quantumcomputinglab/qclab: Qclab v0.1.2, Aug. 2021. doi:10.5281/zenodo.5160555.

[3] D. Camps, R. Van Beeumen, and C. Yang. Quantum fourier transform revisited. *Numerical Linear Algebra with Applications*, 28(1):e2331, 2021. doi:10.1002/nla.2331.

[4] Cirq Developers. Cirq, Dec. 2022. See full list of authors on Github: https://github .com/quantumlib/Cirq/graphs/contributors. `doi:10.5281/zenodo.7465577`.

[5] D. Coppersmith. An approximate fourier transform useful in quantum factoring, 1994.

[6] S. Efthymiou, M. Lazzarin, A. Pasquale, and S. Carrazza. Quantum simulation with just-in-time compilation. *Quantum*, 6:814, Sept. 2022. `doi:10.22331/q-2022-09-22-814`.

[7] S. Efthymiou, S. Ramos-Calderer, C. Bravo-Prieto, A. Pérez-Salinas, D. García-Martín, A. Garcia-Saez, J. I. Latorre, and S. Carrazza. Qibo: a framework for quantum simulation with hardware acceleration. *Quantum Science and Technology*, 7(1):015018, dec 2021. `doi:10.1088/2058-9565/ac39f5`.

[8] L. Fang, ahehn nv, hhbayraktar, and sam stanwyck. Nvidia/cuquantum: cuquantum python v22.11.0.1, Jan. 2023. `doi:10.5281/zenodo.7523366`.

[9] T. Jones, A. Brown, I. Bush, and S. C. Benjamin. QuEST and high performance simulation of quantum computers. *Scientific Reports*, 9(1), July 2019. `doi:10.1038/s41598-019-47174-9`.

[10] H. Liu, G. H. Low, D. S. Steiger, T. Häner, M. Reiher, and M. Troyer. Prospects of quantum computing for molecular sciences. *Materials Theory*, 6(1), Mar. 2022. `doi:10.1186/s41313-021-00039-z`.

[11] Qiskit Developers. Qiskit: An open-source framework for quantum computing, 2021. `doi:10.5281/zenodo.2573505`.

[12] Quantum AI team. Suppressing quantum errors by scaling a surface code logical qubit. *Nature*, 614(7949):676–681, Feb. 2023. `doi:10.1038/s41586-022-05434-1`.

[13] Quantum AI team and collaborators. qsim, Sept. 2020. `doi:10.5281/zenodo.4023103`.

[14] C. Ryan-Anderson et al. Implementing fault-tolerant entangling gates on the five-qubit code and the color code, 2022. `doi:10.48550/arXiv.2208.01863`.

[15] R. Van Beeumen and D. Camps. Quantumcomputinglab/qclabpp: Qclab++ v0.1.2, Aug. 2021. `doi:10.5281/zenodo.5160682`.

[16] H. J. Williams. Versatile neutral atoms take on quantum circuits. *Nature*, 604(7906):429–430, Apr. 2022. `doi:10.1038/d41586-022-01029-y`.